Journal of MATERIALS RESEARCH

Article
DOI: 10.1557/jmr.2019.356

ATOMIC LAYER DEPOSITION FOR EMERGING THIN-FILM MATERIALS AND APPLICATIONS

FOCUS ISSUE

Nanoscale Al_2O_3 coating to stabilize selenium cathode for sodium–selenium batteries

Mohammad Hossein Aboonasr Shiraz[1], Hongzheng Zhu[1], Jian Liu[1,a)]

[1]School of Engineering, Faculty of Applied Science, University of British Columbia, Kelowna BC V1V 1V7, Canada
[a)]Address all correspondence to this author. e-mail: Jian.liu@ubc.ca

Received: 1 October 2019; accepted: 4 November 2019

Na–Se batteries are promising energy storage systems for grid and transportation applications, due to the high volumetric energy density and relatively low cost. However, the development of Na–Se batteries has been hindered by the shuttle effect originating from polyselenide dissolution from the Se cathode. Herein, we reported the utilization of nanoscale Al_2O_3 surface coating by atomic layer deposition (ALD) to protect a microporous carbon/Se (MPC/Se) cathode and reduce polyselenide dissolution. Compared with the pristine MPC/Se, Al_2O_3-coated MPC/Se cathode exhibited improved discharge capacity, cycling stability, and rate capability in Na–Se batteries. Post-cycling analysis disclosed that Al_2O_3 coating on MPC/Se cathode effectively suppressed the polyselenide dissolution, facilitated the formation of thin and stable solid electrolyte interphase (SEI) layers, and reduced charge transfer resistance, thus improving the overall performance of Na–Se batteries. This work suggests the effectiveness of interface control by ALD in enabling high-performance Na–Se batteries and might shed light on the development of new-generation Li/Na/K-chalcogenide batteries.

Introduction

Lithium-ion batteries (LIBs) have made a revolution in portable electronic devices over decades and have been used in electric vehicles, hybrid electric vehicles, and grid energy storage systems due to their long cycle life and high energy density [1]. However, LIBs using intercalation chemistry are gradually approaching their theoretical limit, and cannot meet the increasing demand for higher energy density and lower cost from end users in automotive industry and stationary applications [2]. Therefore, it becomes imperative to develop new-generation battery technologies that satisfy these requirements. Among various potential systems, sodium–selenium (Na–Se) batteries have drawn much attention, because of the large abundance and low cost of sodium and decent energy density of Se [3]. As a cathode material, Se provides a moderate gravimetric capacity of 678 mA h/g and a high volumetric capacity of 3270 mA h/cm^3 and possesses a high electronic conductivity of 1×10^{-3} S/m (versus 5×10^{-28} S/m for S) [4, 5, 6]. These advantages of Se have stimulated growing research in developing Li–Se and Na–Se batteries over the past years.

Na–Se batteries are still in their infant stage and face a significant challenge, i.e., shuttle effect, which was caused by polyselenide dissolution from Se cathodes. Shuttle effect not only leads to the loss of active Se material but also results in the corrosion of Na metal anode, causing low Coulombic efficiency (CE) and rapid performance decay in Na–Se batteries [4, 5, 6, 7]. To date, several approaches have been developed to address shuttle effect problem, and the confinement of Se into porous carbon matrix is one of the most promising strategies [8, 9, 10, 11, 12, 13, 14]. For example, Wang and co-workers prepared Se/mesoporous carbon at 600 °C under vacuum, and the Se/mesoporous carbon cathode delivered a specific capacity of 340 mA h/g after 380 cycles in Na–Se batteries [13]. Moreover, several recent works have explored various metal organic frameworks (MOF) (such as zinc-glutamate MOF, ZIF-67, and ZIF-8) [15, 16, 17] as starting materials to synthesize porous carbon as hosts for Se cathodes in Na–Se batteries. Although the space confinement has been effective in improving the overall performance of Se cathode, polyselenide dissolution still occurs in Na–Se batteries using porous carbon confined Se cathode. In general, Na–Se batteries show more severe shuttle effect than their Li–Se counterparts [6]. For Li–Se batteries using carbonate-based electrolytes, Se undergoes a one-step reaction from Se to Li_2Se, without the formation

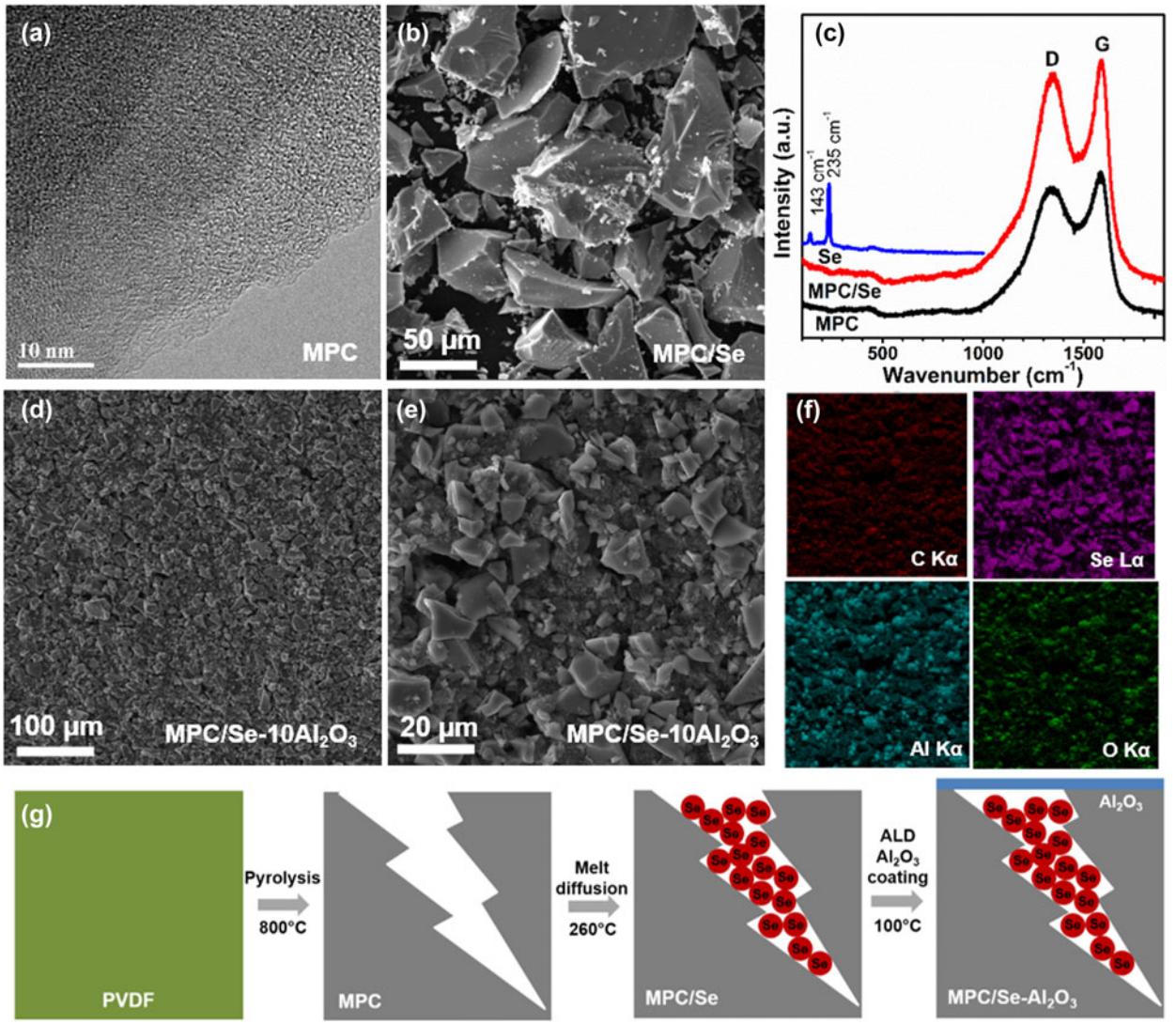

Figure 1: (a) HRTEM image of MPC; (b) SEM image of MPC/Se; (c) Raman spectra of MPC, MPC/Se, and bulk Se; (d, e) SEM images and (f) EDX elemental mapping of MPC/Se coated with 10 ALD cycle Al_2O_3 (MPC/Se-10Al_2O_3); and (g) schematic illustration of the preparation process for MPC/Se-Al_2O_3.

of soluble polyselenide intermediates and is featured with one single plateau in its charge–discharge curves [4, 8]. However, for Na–Se batteries, Goodenough and co-workers [19] found that during the first discharge process, Se in microporous carbon (MPC) underwent stepwise reduction to Na_2Se, with the formation of soluble intermediate polyselenides (Na_2Se_x) in Na–Se batteries. One main reason could be due to the larger ionic radius of Na^+ (102 pm) than that of Li^+ (74 pm), which might cause larger volume change in the Se cathode and alter reaction pathways of Se in Na-based batteries [18, 19]. Therefore, it is necessary to develop and use multiple strategies to stabilize Se cathode for high-performance Na–Se batteries.

In addition to the space confinement strategy, surface coating has also been explored as an effective approach to address the shuttle effect problem in S-based [20, 21, 22, 23] and Se-based batteries [24, 25]. Ideally, the surface coating layer should be thin and uniform to reduce the dissolution of intermediate products, while allowing fast Li ion and electron diffusion. In recent years, atomic layer deposition (ALD) has emerged as a powerful technique to realize uniform surface coatings on the anode and cathode for LIBs [26, 27, 28] and next-generation batteries (such as Na-ion, Li–S) [29, 30], to prevent unwanted interfacial reactions and improve the overall performance of batteries. Compared with other coating techniques, ALD provides precise control over the thickness of thin films at the nanoscale level and excellent uniformity on even high aspect ratio substrates [31, 32], promising it great potential for surface and interface engineering in various battery systems. However, the potential of ALD for interface design in Na–Se batteries is yet to be fully exploited.

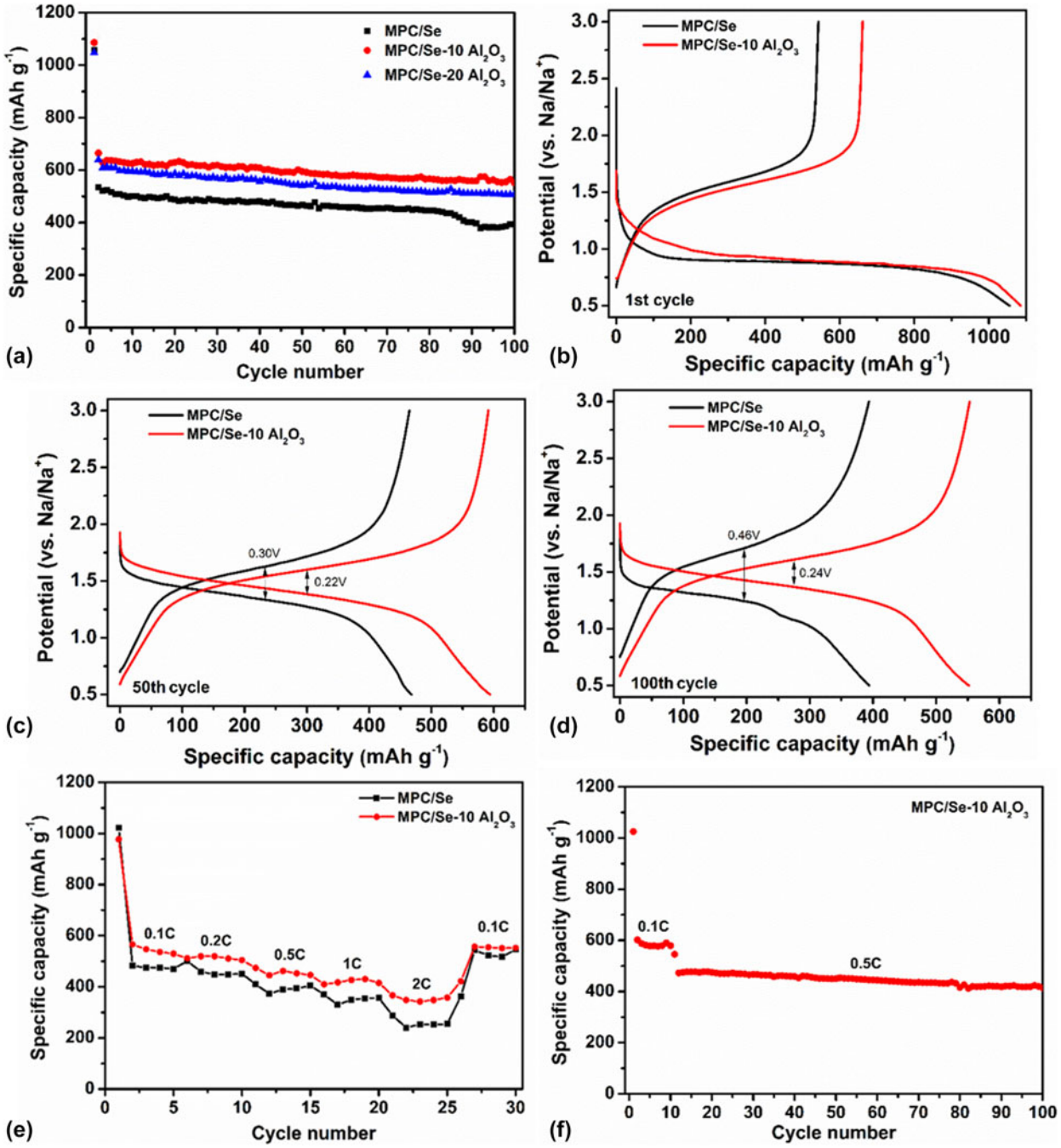

Figure 2: (a) Cycling performance of MPC/Se, MPC/Se-10Al_2O_3, and MPC/Se-20Al_2O_3 measured at 0.1 C (1 C = 678 mA/g); charge–discharge profiles of MPC/Se and MPC/Se-10Al_2O_3 in the (b) 1st cycle, (c) 50th cycle, and (d) 100th cycle; (e) rate capability of MPC/Se and MPC/Se-10Al_2O_3; (f) cycling stability of MPC/Se-10Al_2O_3 tested at 0.1 C in the first 10 cycles and 0.5 C afterward. The electrolyte is 1 M $NaClO_4$, EC:DEC + 3% FEC.

Herein, we reported the utilization of nanoscale Al_2O_3 surface coating by ALD to stabilize the Se cathode for high-performance Na–Se batteries with carbonate-based electrolytes. MPC prepared by pyrolysis of polyvinylidene fluoride (PVDF) was adopted to fabricate MPC/Se cathode. It was found that Al_2O_3 surface coating effectively suppressed the polyselenide dissolution from the MPC/Se cathode, thus reducing the loss of Se active material and improving the overall performance of Na–Se batteries.

Results and discussion

MPC was synthesized by the direct pyrolysis of PVDF at 800 °C in a nitrogen environment and used as the Se host without any further activation process. Previous work has shown that MPC prepared at this condition exhibited the highest surface area and dominant microporous feature, which were important merits for confining Se in the cathode [33, 34, 35]. High-

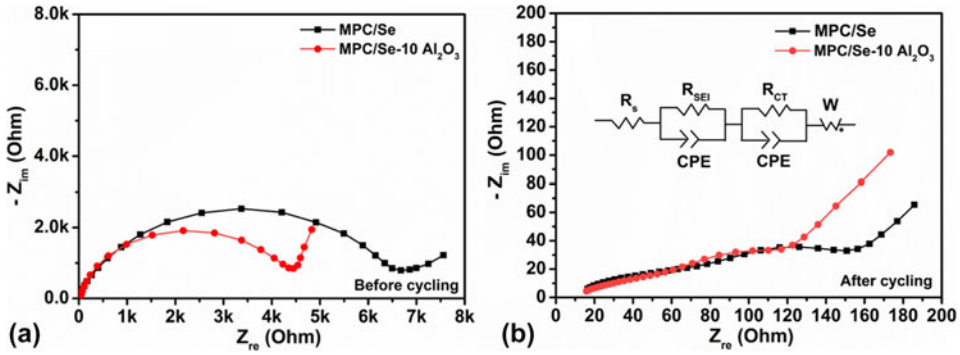

Figure 3: The Nyquist profiles of MPC/Se and MPC/Se-10Al_2O_3 (a) before cycling and (b) after 100 cycles (inset shows the equivalent circuit used to fit the Nyquist plots).

TABLE I: EIS parameters obtained by fitting the Nyquist plots of MPC/Se and MPC/Se-10Al_2O_3 after 100 cycles.

Sample after cycling	R_s (Ω)	R_{SEI} (Ω)	R_{CT} (Ω)
MPC/Se	6.7	40.9	90.6
MPC/Se-10Al_2O_3	8.4	20.2	68.6

resolution transmission electron microscopy (HRTEM) characterization discloses the disordered structure of the as-synthesized MPC [Fig. 1(a)]. After the Se impregnation, MPC/Se composite displays irregular shapes with particle sizes of about 10–200 μm [Fig. 1(b)]. Raman spectra of MPC and MPC/Se [Fig. 1(c)] show two vibration peaks at about 1350 and 1600 cm^{-1}, which are assigned to D band (disordered carbon originating from sp^3 carbons) and G band (hexagonal carbon), respectively [36, 37]. It should be noted that MPC/Se composite displays no obvious peaks at 143 and 235 cm^{-1} for crystalline bulk Se [38]. Raman analysis reveals that there is no bulk Se in the MPC/Se composite, and all Se are mainly encapsulated in the micropores of MPC. Se content in MPC/Se composite was determined to be 48 wt% by thermogravimetric analysis. Al_2O_3 coating was deposited on the MPC/Se electrode by ALD using 10 cycles and 20 cycles, and the prepared samples were designated as MPC/Se-10Al_2O_3 and MPC/Se-20Al_2O_3, respectively. As seen in Figs. 1(d) and 1(e), MPC/Se-10Al_2O_3 retains the morphology of MPC/Se and turns into slightly darker in the scanning electron microscope (SEM) image due to non-conductive nature of Al_2O_3 coating (as also shown for MPC/Se–20Al_2O_3 and MPC/Se-100Al_2O_3 in Fig. SI-1). Elemental mapping by energy-dispersive X-ray spectroscopy (EDS) in Fig. 1(f) shows the uniform distribution of Al and O elements on the surface of MPC/Se cathode. The thickness of Al_2O_3 on MPC/Se-10Al_2O_3 and MPC/Se-20Al_2O_3 is about 1 nm and 2 nm, respectively, based on the growth rate of Al_2O_3 on standard Si wafers [31, 32]. The preparation process for MPC/Se-Al_2O_3 is illustrated in Fig. 1(g).

The influence of Al_2O_3 coating on electrochemical performance of MPC/Se cathode is studied in Na–Se batteries between 0.5 and 3 V at 0.1 C, and the results are shown in Fig. 2. As shown in Fig. 2(a), MPC/Se-10Al_2O_3 and MPC/Se-20Al_2O_3 exhibit an initial capacity of about 1050 mA h/g, similar to the pristine MPC/Se. After the 1st cycle, however, there is a dramatic difference in the specific capacity of the MPC/Se cathodes with and without Al_2O_3 coating. The discharge capacity in the 2nd cycle was 534 mA h/g, 664 mA h/g, and 639 mA h/g for MPC/Se, MPC/Se-10Al_2O_3 and MPC/Se-20Al_2O_3, respectively. The capacity drop from the 1st cycle to the 2nd one in all the three samples could be ascribed to the formation of SEI film and the decomposition of electrolytes on the MPC/Se cathode [13]. For MPC/Se cathode, the capacity decreases gradually from 534 mA h/g in the 2nd cycle to 446 mA h/g after 80 cycles and then undergoes rapid decay to 396 mA h/g until 100 cycles. In contrast, MPC/Se-10Al_2O_3 could still deliver a specific capacity of 570 mA h/g after 100 cycles. The capacity retention of MPC/Se cathode from the 2nd cycle to 100th cycle was elevated from 73 to 86% by using Al_2O_3 coating. Moreover, the specific capacity and cycling performance of MPC/Se-20Al_2O_3 are lower than those of MPC/Se-10Al_2O_3 but better than those of pristine MPC/Se cathode. The thickness of Al_2O_3 coating on Se/MPC cathode was also optimized in 1 M $NaClO_4$ and ethylene carbonate/diethyl carbonate (EC:DEC) without fluoroethylene carbonate additive (Fig. SI-2). Further increase in Al_2O_3 coating more than 20 cycles causes an obvious decrease in the specific capacity. The reason could be due to the insulating nature of Al_2O_3 coating, which might slow down the diffusion of Li ions through the SEI layer [26, 27, 28, 29]. This result suggests the importance of Al_2O_3 coating thickness for achieving optimal protection effect in Se cathodes.

Figures 2(b)–2(d) present charge/discharge curves of the MPC/Se and MPC/Se-10Al_2O_3 in the 1st, 50th, and 100th cycle tested at 0.1 C. As shown in Fig. 2(b), both MPC/Se and MPC/Se-10Al_2O_3 exhibit one obvious plateau during the discharge and charge process, which is characteristic of micropore-confined Se [13, 14, 15, 16, 17]. CE in the 1st cycle is calculated

https://doi.org/10.1557/jmr.2019.356 Published online by Cambridge University Press

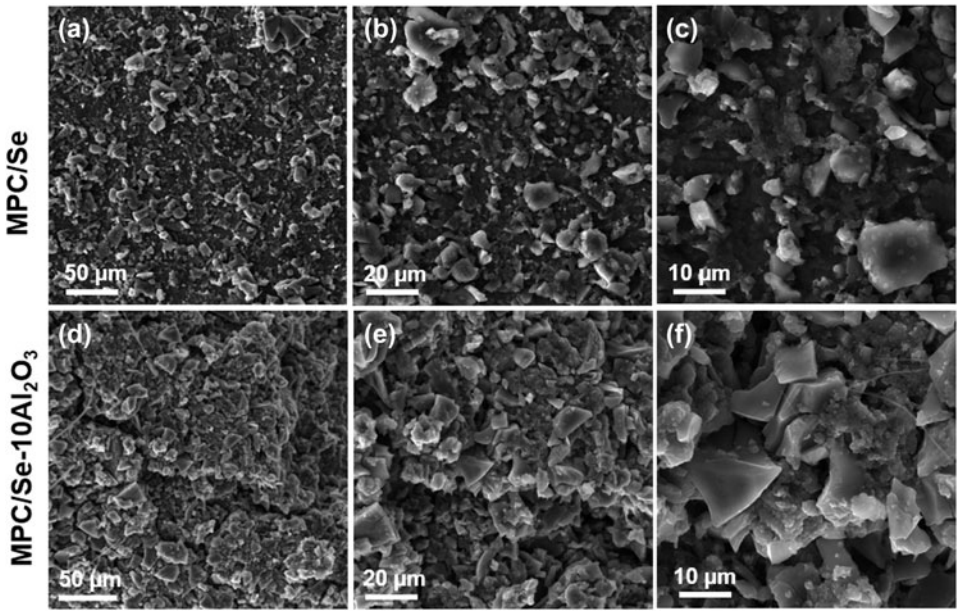

Figure 4: SEM images of (a–c) MPC/Se electrode and (d–f) MPC/Se-10Al_2O_3 electrode after 100 cycles.

to be 51.4% and 60.9% for MPC/Se and MPC/Se-10Al_2O_3, respectively, implying that Al_2O_3 coating reduces the side reaction between Se electrode and the electrolyte. Moreover, it is found from Figs. 2(b)–2(d) that Al_2O_3 coating also minimizes the polarization of MPC/Se cathode during the discharge and charge process. For example, midpoint-voltage differences in the 50th and 100th cycles are 0.30 and 0.46 V for MPC/Se and 0.22 and 0.24 V for MPC/Se-10Al_2O_3 [Figs. 2(c) and 2(d)], indicating enhanced reaction kinetics of MPC/Se by Al_2O_3 coating. The improved capacity and kinetics in MPC/Se-10Al_2O_3 could be resulted from the protective effect of nanoscale Al_2O_3 coating, which alleviates polyselenide dissolution and reduces the deposition of solid polyselenides. Moreover, a previous study on Na-ion batteries has shown that the Al_2O_3 coating on the electrode might convert to a stable Na–Al–O layer, which served as a Na buffer layer to facilitate Na ion diffusion [39, 40]. As a result of the improved kinetics, the MPC/Se-10Al_2O_3 also exhibits better rate capability than MPC/Se cathode [Fig. 2(e)]. MPC/Se-10Al_2O_3 could deliver a specific capacity of 544.4 mA h/g, 518.5 mA h/g, 458.3 mA h/g, 422.5 mA h/g, and 343.8 mA h/g at 0.1 C, 0.2 C, 0.5 C, 1 C, and 2 C, respectively, while MPC/Se shows a specific capacity of 477.7 mA h/g, 463.3 mA h/g, 370.1 mA h/g, 353.3 mA h/g, and 245.7 mA h/g under the same condition. At last, the cycling test at 0.5 C shows that MPC/Se-10Al_2O_3 can maintain a specific capacity of 320 mA h/g after 100 cycles [Fig. 2(f)]. From the results in Fig. 2, it can be concluded that ALD Al_2O_3 coating effectively improves the specific capacity, cycling stability, and rate capability of the MPC/Se cathode in Na–Se batteries.

To find out the underlying mechanism for performance improvement by ALD Al_2O_3 coating, electrochemical impedance spectroscopy (EIS) measurement was performed on MPC/Se and MPC/Se-10Al_2O_3 before and after 100 cycles, and the results are presented in Fig. 3. As seen in Fig. 3(a), both MPC/Se and MPC/Se-10Al_2O_3 display one semicircle in the high-frequency region, which corresponds to the charge transfer resistance (R_{CT}) at the electrode–electrolyte interface, and one inclined line in the low-frequency region, which is interpreted as the finite length Warburg impedance [41]. The smaller R_{CT} in MPC/Se-10Al_2O_3 might be due to the improved physical contact between the electrode material and Al current collector by ultrathin Al_2O_3 coating directly on the electrode, which allows faster electron diffusion [42]. The Nyquist profiles of MPC/Se and MPC/Se-10Al_2O_3 after cycling present one semicircle (R_{CT}) in the high-frequency region, Warburg impedance in the low-frequency domain, and another semicircle in the medium-frequency region, which can be assigned to the Li-ion diffusion resistance at the SEI (R_{SEI}) [41]. The Nyquist profiles are fitted by using the equivalent circuit inserted in Fig. 3(b) to obtain EIS parameters for MPC/Se and MPC/Se-10Al_2O_3 (Table I). From Table I, it is evident that R_{SEI} reduces from 40.9 to 20.2 Ω, while R_{CT} decreases from 90.6 to 68.6 Ω for the MPC/Se cathode with Al_2O_3 coating. EIS analysis clearly indicates that Al_2O_3 surface coating positively affects the formation of SEI layers and reduce charge transfer and Li-ion diffusion resistances on the MPC/Se cathode.

The morphologies of MPC/Se and MPC/Se-10Al_2O_3 after 100 cycles are examined, and the typical SEM images are depicted in Fig. 4. From Figs. 4(a)–4(c), it can be found that the cycled MPC/Se electrode is covered with thick SEI layers and has much less porosity than the uncycled one. The thick SEI layers could originate from the decomposition of electrolytes

https://doi.org/10.1557/jmr.2019.356 Published online by Cambridge University Press

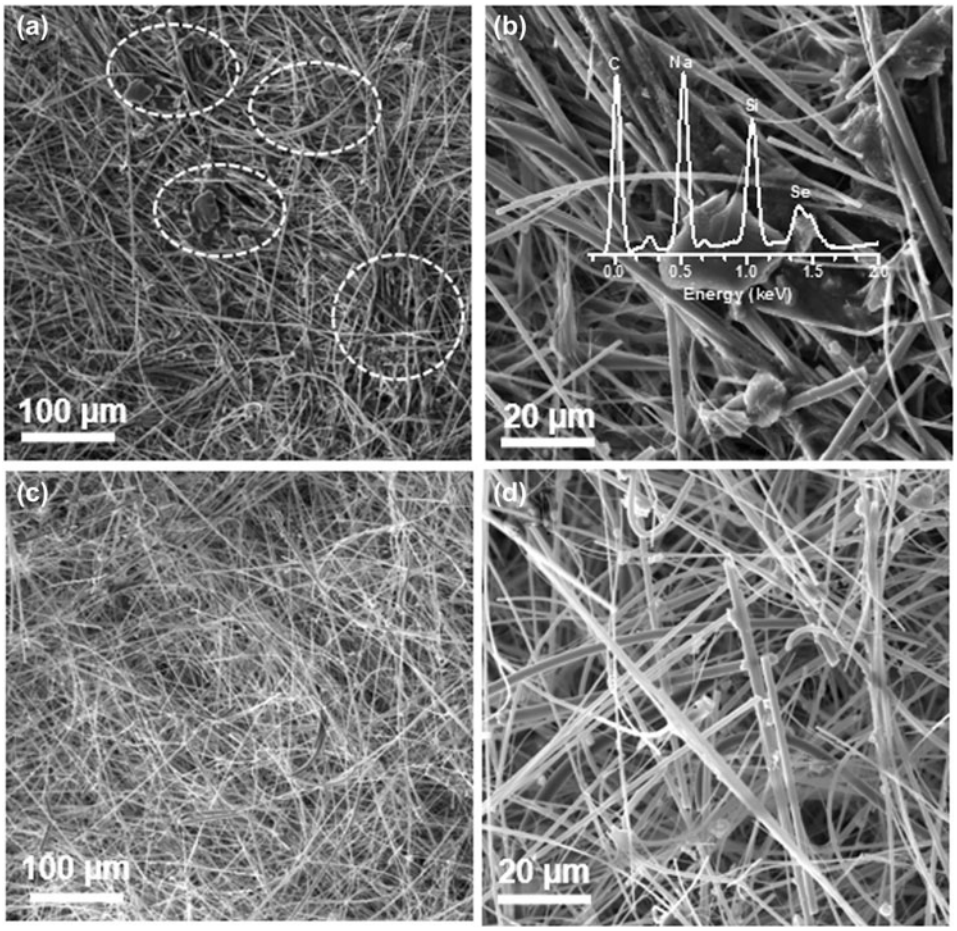

Figure 5: SEM images of glass fibers recycled after 100 cycles from (a, b) the MPC/Se cell and (c, d) the MPC/Se-10Al_2O_3 cell [inset in (b) shows the EDX spectrum of the solid particles].

and the deposit of solid polyselenides (Na_2Se and Na_2Se_2) on MPC/Se surface due to shuttle effect. In contrast, the cycled MPC/Se-10Al_2O_3 cathode possesses much thinner SEI layers. As a result, the sharp edges in the MPC/Se particles are still visible [Fig. 4(f)] compared with these before battery cycling [Fig. 1(e)]. EIS and post-cycling analysis suggest that nanoscale Al_2O_3 surface coating facilitates the formation of robust and thin SEI layers on the MPC/Se electrode, which are believed to account for the reduced R_{CT} and Na-ion diffusion resistance at the electrode–electrolyte interface.

Glass fibers recovered from cycled MPC/Se and MPC/Se-10Al_2O_3 cells are further examined to understand the polyselenide dissolution, and the typical SEM pictures are shown in Fig. 5. Glass fiber facing to the MPC/Se electrode is deposited with micro-sized solid particles [circled in Fig. 5(a)]. EDX analysis confirms strong signals from Na and Se elements, implying that the solid particles might be Na_2Se and/or Na_2Se_2. In contrast, glass fiber from the MPC/Se-10Al_2O_3 cell retains their original fibrous structure and shows no obvious large solid deposits [Figs. 5(c) and 5(d)]. Figure 5 provides an additional evidence for the suppressed polyselenide dissolution from the MPC/Se cathode by Al_2O_3 surface coating.

Conclusions

ALD nanoscale Al_2O_3 surface coating was successfully applied to solve polyselenide dissolution problem and enable MPC/Se cathode for stable and high-capacity Na–Se batteries. The thickness of Al_2O_3 coating had a profound influence on the overall performance of MPC/Se cathode. The optimal electrochemical performance of MPC/Se cathode was achieved by using 10 ALD cycles of Al_2O_3 coating. Al_2O_3-coated MPC/Se cathode exhibited a reversible discharge capacity of 664 mA h/g in the 2nd cycle and 570 mA h/g after 100 cycles. Moreover, Al_2O_3 coating on MPC/Se cathode also improved the rate capability and reduced the polarization during charge/discharge processes. The enhanced performance was due to that nanoscale Al_2O_3 coating suppressed the dissolution of polyselenides, induced the formation of stable and thin SEI layers, and thus decreased the R_{CT} at the electrode–electrolyte interface.

https://doi.org/10.1557/jmr.2019.356 Published online by Cambridge University Press

Methodology

Preparation of MPC, MPC/Se, and MPC/Se-Al_2O_3

PVDF [$(-CH_2CF_2-)_n$, MW: 64.035 g/mol; Alfa Aesar] was put into a tube furnace (Lindberg/Blue M Mini-Mite™) and heated up to the temperature of 800 °C with a heating rate of 10 °C/min and kept for 1 h under the inert gas environment (nitrogen 99.999%) to perform the pyrolysis. The thermal decomposition of PVDF led to the formation of micropores in MPC structure. Black products collected after pyrolysis were MPC and no further activation on MPC was required. The MPC/Se composite was prepared by a melting diffusion method. Briefly, in a mortar, sublimed selenium powder, −100 mesh (99.5%; Sigma-Aldrich), and MPC with the same weight ratio of 50:50 were mixed with each other for 1 h and sealed in a 50 mL stainless steel autoclave. This process was conducted in a glove box workstation under the protection of argon atmosphere with H_2O and O_2 levels below 0.1 ppm. The autoclave was put into a furnace followed by heat treatment at 260 °C for 12 h. The melting diffusion method used the capillary force to diffuse Se into microspores of MPC. To obtain the cathode electrode, 80 wt% of MPC/Se composite, 10 wt% of carbon black (MTI Co.), and 10 wt% of sodium alginate (0.5 wt% aqueous solution; Ward's Science Co., Ltd.) were mixed in planetary mortar to form a uniform slurry, which was then pasted to an Al foil current collector by using a doctor blade. The electrode was kept at room temperature (RT) overnight for initial water evaporation and then underwent complete drying in a vacuum oven at 60 °C for 12 h. Subsequently, the electrode was cut into round disks with a diameter of 12.7 mm for coin-cell assembly.

The coating of Al_2O_3 on MPC/Se electrode was performed at 100 °C by alternatively supplying trimethylamine (TMA) and H_2O into a commercial ALD reactor (GEMStar™ XT Atomic Layer Deposition Systems; Arradiance). Thickness of Al_2O_3 on MPC/Se cathode was adjusted by using 10 and 20 ALD cycles, and the prepared sample was designated as MPC/Se-10Al_2O_3 and MPC/Se-20Al_2O_3, respectively.

Structural and electrochemical characterizations of MPC and MPC/Se composites

SEM equipped with EDS (Tescan MIRA3) was used to examine the morphology and structure of different samples. The electrochemical properties of the MPC/Se composites were evaluated in CR 2032 coin cells by using Na foil as the counter electrode. The assembly of coin cells was performed in a glove box workstation with argon protecting gas (99.999%). Each coin cell was composed of one MPC/Se electrode as the cathode, Na metal as the anode, and glass fiber as the separator. The electrolyte was 1 M $NaClO_4$ in a mixture of EC/DEC (1:1 v/v) with 3 vol% FEC additive. The cycling performance of the coin cells was tested in a voltage window of 0.5–3 V on a Neware BTS 4000 battery testing system.

Acknowledgments

This work was supported by the Nature Sciences and Engineering Research Council of Canada (NSERC), Canada Foundation for Innovation (CFI), BC Knowledge Development Fund (BCKDF), and the University of British Columbia (UBC).

Supplementary material

To view supplementary material for this article, please visit https://doi.org/10.1557/jmr.2019.356

References

1. **J-M. Tarascon and M. Armand**: Issues and challenges facing rechargeable lithium batteries. *Nature* **414**, 359 (2001).
2. **M.M. Thackeray, C. Wolverton, and E.D. Isaacs**: Electrical energy storage for transportation—Approaching the limits of, and going beyond, lithium-ion batteries. *Energy Environ. Sci.* **5**, 7854 (2012).
3. **A. Abouimrane, D. Dambournet, K.W. Chapman, P.J. Chupas, W. Weng, and K. Amine**: A new class of lithium and sodium rechargeable batteries based on selenium and selenium–sulfur as a positive electrode. *J. Am. Chem. Soc.* **134**, 4505 (2012).
4. **G-L. Xu, J. Liu, R. Amine, Z. Chen, and K. Amine**: Selenium and selenium-sulfur chemistry for rechargeable lithium batteries: Interplay of cathode structures, electrolytes, and interfaces. *ACS Energy Lett.* **2**, 605 (2017).
5. **C-P. Yang, Y-X. Yin, and Y-G. Guo**: Elemental selenium for electrochemical energy storage. *J. Phys. Chem. Lett.* **6**, 256 (2015).
6. **X. Gu, T. Tang, X. Liu, and Y. Hou**: Rechargeable metal batteries based on selenium cathodes: Progress, challenges and perspectives. *J. Mater. Chem. A* **19**, 11566 (2019).
7. **F. Li, Z. Wei, A. Manthiram, Y. Feng, and J. Ma**: Sodium-based batteries: From critical materials to battery systems. *J. Mater. Chem. A* **7**, 9406 (2019).
8. **L. Zeng, W. Zeng, Y. Jiang, X. Wei, W. Li, C. Yang, Y. Zhu, and Y. Yu**: A flexible porous carbon nanofibers-selenium cathode with superior electrochemical performance for both Li–Se and Na–Se batteries. *Adv. Energy Mater.* **5**, 1401377 (2015).
9. **Q. Li, H. Liu, Z. Yao, J. Cheng, T. Li, Y. Li, C. Wolverton, J. Wu, and V.P. Dravid**: Electrochemistry of selenium with sodium and lithium: Kinetics and reaction mechanism. *ACS Nano* **10**, 8788–8795 (2016).
10. **J. Ding, H. Zhou, H. Zhang, T. Stephenson, Z. Li, D. Karpuzov, and D. Mitlin**: Exceptional energy and new insight with a sodium–

selenium battery based on a carbon nanosheet cathode and a pseudographite anode. *Energy Environ. Sci.* **10**, 153 (2017).

11. **C. Luo, J. Wang, L. Suo, J. Mao, X. Fan, and C. Wang**: In situ formed carbon bonded and encapsulated selenium composites for Li–Se and Na–Se batteries. *J. Mater. Chem. A* **3**, 555 (2015).
12. **H. Wang, Y. Jiang, and A. Manthiram**: N-doped Fe_3C@C as an efficient polyselenide reservoir for high-performance sodium-selenium batteries. *Energy Storage Mater.* **16**, 374 (2019).
13. **C. Luo, Y. Xu, Y. Zhu, Y. Liu, S. Zheng, Y. Liu, A. Langrock, and C. Wang**: Selenium@mesoporous carbon composite with superior lithium and sodium storage capacity. *ACS Nano* **7**, 8003 (2013).
14. **Y. Yao, M. Chen, R. Xu, S. Zeng, H. Yang, S. Ye, F. Liu, X. Wu, and Y. Yu**: CNT interwoven nitrogen and oxygen dual-doped porous carbon nanosheets as free-standing electrodes for high-performance Na–Se and K–Se flexible batteries. *Adv. Mater.* **30**, 1805234 (2018).
15. **W. Dong, H. Chen, F. Xia, W. Yu, J. Song, S. Wu, Z. Deng, Z.Y. Hu, T. Hasan, Y. Li, H. Wang, L. Chen, and B.L. Su**: Selenium clusters in Zn-glutamate MOF derived nitrogen-doped hierarchically radial-structured microporous carbon for advanced rechargeable Na–Se batteries. *J. Mater. Chem. A* **6**, 22790 (2018).
16. **X. Yang, S. Wang, D.Y.W. Yu, and A. Rogach**: Direct conversion of metal-organic frameworks into selenium/selenide/carbon composites with high sodium storage capacity. *Nano Energy* **58**, 392 (2019).
17. **Q. Xu, T. Liu, Y. Li, L. Hu, C. Dai, Y. Zhang, Y. Li, D. Liu, and M. Xu**: Selenium encapsulated into metal–organic frameworks derived N-doped porous carbon polyhedrons as cathode for Na–Se batteries. *ACS Appl. Mater. Interfaces* **9**, 41339 (2017).
18. **L. Wang, X. Zhang, L. Deng, J. Tang, H. Deng, W. Hu, and Z. Liu**: Revealing the reaction mechanism of sodium selenide confined within a single-walled carbon nanotube: Implications for Na–Se batteries. *ACS Appl. Mater. Interfaces* **11**, 4995 (2019).
19. **S. Xin, L. Yu, Y. You, H.P. Cong, Y.X. Yin, X.L. Du, Y.G. Guo, S.H. Yu, Y. Cui, and J.B. Goodenough**: The electrochemistry with lithium versus sodium of selenium confined to slit micropores in carbon. *Nano Lett.* **16**, 4560 (2016).
20. **S.Z. Wei, W. Li, J.J. Cha, G. Zheng, Y. Yang, M.T. McDowell, P.C. Hsu, and Y. Cui**: Sulphur-TiO_2 yolk–shell nanoarchitecture with internal void space for long-cycle lithium–sulphur batteries. *Nat. Commun.* **4**, 1331 (2013).
21. **K.T. Lee, R. Black, T. Yim, X. Ji, and L.F. Nazar**: Surface-initiated growth of thin oxide coatings for Li–sulfur battery cathodes. *Adv. Energy Mater.* **2**, 1490 (2012).
22. **W. Li, Q. Zhang, G. Zheng, Z.W. Seh, H. Yao, and Y. Cui**: Understanding the role of different conductive polymers in improving the nanostructured sulfur cathode performance. *Nano Lett.* **13**, 5534 (2013).
23. **X. Li, J. Liu, B. Wang, M.N. Banis, B. Xiao, R. Li, T.K. Sham, and X. Sun**: Nanoscale stabilization of Li–sulfur batteries by atomic layer deposited Al_2O_3. *RSC Adv.* **4**, 27126 (2014).
24. **F. Zhang, P. Xiong, X. Guo, J. Zhang, W. Yang, W. Wu, H. Liu, and G. Wang**: A nitrogen, sulphur dual-doped hierarchical porous carbon with interconnected conductive polyaniline coating for high-performance sodium–selenium batteries. *Energy Storage Mater.* **19**, 251 (2019).
25. **D. Ma, Y. Li, J. Yang, H. Mi, S. Luo, L. Deng, C. Yan, P. Zhang, Z. Lin, and X. Ren**: Atomic layer deposition-enabled ultrastable freestanding carbon–selenium cathodes with high mass loading for sodium–selenium battery. *Nano Energy* **43**, 317 (2018).
26. **J. Liu and X. Sun**: Elegant design of electrode and electrode/electrolyte interface in lithium-ion batteries by atomic layer deposition. *Nanotechnology* **26**, 024001 (2015).
27. **W. Lu, L. Liang, X. Sun, X. Sun, C. Wu, L. Hou, J. Sun, and C. Yuan**: Recent progresses and development of advanced atomic layer deposition towards high-performance Li-ion batteries. *Nanomaterials* **7**, 325 (2017).
28. **H.C.M. Knoops, M.E. Donders, M.C.M. van de Sanden, P.H.L. Notten, and W.M.M. Kessels**: Atomic layer deposition for nanostructured Li-ion batteries. *J. Vac. Sci. Technol., A* **30**, 010801 (2012).
29. **X. Meng**: Atomic-scale surface modifications and novel electrode designs for high-performance sodium-ion batteries via atomic layer deposition. *J. Mater. Chem. A* **5**, 10127 (2017).
30. **B. Yan, X. Li, Z. Bai, X. Song, D. Xiong, M. Zhao, D. Li, and S. Lu**: A review of atomic layer deposition providing high performance lithium sulfur batteries. *J. Power Sources* **338**, 34 (2017).
31. **S.M. George**: Atomic layer deposition: An overview. *Chem. Rev.* **110**, 111 (2010).
32. **V. Miikkulainen, M. Leskelä, M. Ritala, and R.L. Puurunen**: Crystallinity of inorganic films grown by atomic layer deposition: Overview and general trends. *J. Appl. Phys.* **113**, 021301 (2013).
33. **B. Xu, S. Hou, M. Chu, G. Cao, and Y. Yang**: An activation-free method for preparing microporous carbon by the pyrolysis of poly(vinylidene fluoride). *Carbon* **48**, 2812 (2010).
34. **B. Xu, S. Hou, H. Duan, G. Cao, M. Chu, and Y. Yang**: Ultramicroporous carbon as electrode material for supercapacitors. *J. Power Sources* **228**, 193 (2013).
35. **M.H. Aboonasr Shiraz, H. Zhu, Y. Liu, X. Sun, and J. Liu**: Activation-free synthesis of microporous carbon from polyvinylidene fluoride as host materials for lithium-selenium batteries. *J. Power Sources* **438**, 227059 (2019).
36. **C-P. Yang, S. Xin, Y-X. Yin, H. Ye, J. Zhang, and Y-G. Guo**: An advanced selenium-carbon cathode for rechargeable lithium–selenium batteries. *Angew. Chem., Int. Ed.* **52**, 8363 (2013).

37. **Z. Li, L. Yuan, Z. Yi, Y. Liu, and Y. Huang**: Confined selenium within porous carbon nanospheres as cathode for advanced Li–Se batteries. *Nano Energy* **9**, 229 (2014).

38. **R. Fang, G. Zhou, S. Pei, F. Li, and H.M. Cheng**: Localized polyselenides in a graphene-coated polymer separator for high rate and ultralong life lithium–selenium batteries. *Chem. Commun.* **51**, 3667 (2015).

39. **X. Han, Y. Liu, Z. Jia, Y.C. Chen, J. Wan, N. Weadock, K.J. Gaskell, T. Li, and L. Hu**: Atomic-layer-deposition oxide nanoglue for sodium ion batteries. *Nano Lett.* **14**, 1139 (2014).

40. **S.C. Jung, H.J. Kim, J.W. Choi, and Y.K. Han**: Sodium ion diffusion in Al_2O_3: A distinct perspective compared with lithium ion diffusion. *Nano Lett.* **141**, 16559 (2014).

41. **J.T. Lee, H. Kim, N. Nitta, K-S. Eom, D-C. Lee, F. Wu, H-T. Lin, B. Zdyrko, W. Il Chod, and G. Yushin**: Stabilization of selenium cathodes via in situ formation of protective solid electrolyte layer. *J. Mater. Chem. A* **2**, 18898 (2014).

42. **Y.S. Jung, A.S. Cavanagh, L.A. Riley, S.H. Kang, A.C. Dillon, M.D. Groner, S.M. George, and S.H. Lee**: Ultrathin direct atomic layer deposition on composite electrodes for highly durable and safe Li-ion batteries. *Adv. Mater.* **22**, 2172 (2010).